

# GEM: A Dynamic Tracking Model for Mesoscale Eddies in the Ocean

Qiu-Yang Li<sup>1</sup>, Liang Sun<sup>1,2</sup>, Sheng-Fu Lin<sup>1</sup>

<sup>1</sup>School of Earth and Space Sciences, University of Science and Technology of China, 230026, Hefei, China.

<sup>2</sup>State Key Laboratory of Satellite Ocean Environment Dynamics, Second Institute of Oceanography, State Oceanic Administration, Hangzhou, 310012, PR China.

*Correspondence to:* L. Sun ([sunl@ustc.edu.cn](mailto:sunl@ustc.edu.cn))

## Abstract

Genealogical Evolution Model (GEM) is an efficient logical model used to track dynamic evolution of mesoscale eddies in the ocean. It can distinguish different dynamic processes (e.g., merging and splitting) within a dynamic evolution pattern, which is difficult to accomplish using other tracking methods. To this end, GEM first uses a two-dimensional (2-D) similarity vector (i.e. a pair of ratios of overlap area between two eddies to the area of each eddy) rather than a scalar to measure the similarity between eddies, which effectively solves the “missing eddy” problem (temporarily lost eddy in tracking). Second, GEM uses both parents (a new eddy) and children (e.g., splitting eddies from parent eddy) in tracking, and the dynamic processes are described as birth and death of different generations. Additionally, a look-ahead approach with selection rules effectively simplifies computation and recording. All of the computational steps are linear and do not include iteration. Given the pixel number of the target region  $L$ , the maximum number of eddies  $M$ , the number  $N$  of look-ahead time steps, and the total number of time steps  $T$ , the total time complexity is  $O(LM(N+1)T)$ . The tracking of each eddy is very smooth because we require that the snapshots of each eddy on adjacent days overlap one another.

Although eddy splitting or merging is ubiquitous in the ocean, they have different geographic distribution in the Northern Pacific Ocean. Both the merging and splitting rates of the eddies are high, especially at the western boundary, in currents and in “eddy deserts”. GEM is useful not only for satellite-based observational data but also for numerical simulation outputs. It is potentially useful for studying dynamic processes in other related fields, e.g., the dynamics of cyclones in meteorology.

## 29 1 Introduction

30 Eddies are ubiquitous in the ocean, and they move from one place to another [Chelton and Schlax, 1996; Chelton et  
31 al., 2007]. Eddies in the ocean can cause large-scale transports of heat, salt and other tracers [Bennett and White,  
32 1986; Chelton et al., 2011a; Dong et al., 2014; McGillicuddy et al., 2011] by trapping these passive tracers inside the  
33 eddies. Such transports may have important impacts on the environment and climate of the ocean [Dong et al., 2014].  
34 To address various applications in the studies that use satellite products of sea level anomaly (SLA) data [e.g.,  
35 Chelton et al., 2011b] and numerical simulation outputs [e.g., Petersen et al., 2013], oceanic eddies should be  
36 automatically recorded using these data and outputs [e.g., Yang et al., 2013; Sun et al., 2014; Pegliasco et al., 2015].  
37 In general, the recording of oceanic eddies often includes two independent steps: automated eddy identification and  
38 automated eddy tracking. The eddies are identified in a sequence of SLA maps using an identification algorithm or  
39 identified from velocity fields. An automated tracking procedure is then applied to determine the trajectory of each  
40 eddy [Chelton et al., 2011b]. Several automated identification and tracking algorithms have been developed for  
41 eddies in the ocean [Chelton et al., 2011b; Ienna et al., 2014; Mason et al., 2014; Yi et al., 2015].

42 For the eddy tracking stage, according to a recent census [Wang et al., 2015; Yi et al., 2015], approximately 10-30%  
43 of eddies may be found in proximity to a neighboring eddy in any given global SLA map and they frequently  
44 interact. Therefore, an eddy tracking process should have the capability to distinguish different dynamic processes  
45 (e.g., merging and splitting) during its dynamic evolution. Moreover, an eddy tracking process must be accurate and  
46 fast enough to handle a huge amount of data, which will be even larger in size if spatio-temporal resolution of  
47 observations and numerical simulations increases.

48 Implemented automated tracking procedures differ in detail, but they are all similar in concept because they utilize  
49 the nearest neighbor strategy [Chelton et al., 2011b]. For each eddy  $E_i$  identified at time step  $k$ , the nearest eddy to  $E_i$   
50 at the next time step  $k+1$  is identified as part of the trajectory of eddy  $E_i$ . A more advanced procedure uses eddy  
51 shape error as an additional condition when assessing an eddy trajectory [Mason et al., 2014].

52 However, there is a “missing eddy” problem that must be solved in the eddy tracking stage [Chelton et al., 2011b].  
53 An eddy at time step  $k$  may have no associated eddy at time step  $k+1$ , which is simply due to a temporary missing  
54 eddy in the identification process; this can occur for a variety of reasons related to sampling errors and measurement  
55 noise [Chelton et al., 2011b] or limitations of the eddy detection step when an eddy is too weak/small at a time step.  
56 Chelton and his colleagues made an attempt to accommodate such problems; they allowed for the reappearance of a  
57 temporarily missing eddy by looking ahead two or three time steps. Unfortunately, this “look-ahead” procedure  
58 considers too many nearby eddies as potential ones. In practice, the results of this simple “look-ahead” procedure  
59 were disappointing because the resulting eddy trajectories often jumped from one eddy track to another. As a result,  
60 the look-ahead approach was abandoned, even though it is a solution to the “missing eddy” problem [Chelton et al.,  
61 2011b].

62 Recently, the concept of Multiple Hypothesis Assignment (MHA) was introduced to solve the missing eddy problem  
63 by abandoning the simple closest eddy strategy and applying a new “look-ahead” procedure [Faghmous et al., 2013].

64 The MHA method can effectively solve the missing eddy problem in a straight-line model when the trajectory being  
65 followed is a branch without any splitting, but it is algorithmically and computationally complex. Given the  
66 maximum number of eddies in any time frame  $M$ , the number of look-ahead time steps  $N$  (with  $N=0$  being the  
67 original linear closest eddy procedure without look-ahead) and the total number of time steps  $T$ , the MHA has a  
68 larger time complexity (the total amount of time taken by an algorithm),  $O(M^{N+1}T)$  at the worst-case [Faghmous et  
69 al., 2013].

70 The existing straight-line model can trace the kinematic motion of eddy. The dynamic evolutionary processes (e.g.,  
71 merging and splitting) of the eddy are, however, ignored by the model. This implies that each eddy  $E_i$  identified at  
72 time step  $k$  has only one eddy as part of its trajectory at time step  $k-1$  and has only one eddy as part of its trajectory  
73 at time step  $k+1$ . In the ocean, small eddies may merge to form larger ones. As shown in Figure 1, the anticyclonic  
74 eddies AC1 and AC2 observed on July 26, 2006 merged into a single one on July 31, 2006. Then, the cyclonic  
75 eddies C1 and C2 on July 26, 2006 merged to form a larger one on August 3, 2006. To describe such processes, the  
76 eddy tracking records should be trees with branches instead of simple straight lines.

77 To record the dynamic evolution of eddies, two fundamental algorithms are required. First, the two nearby eddies  
78 should be distinguished in the identification stage using a segmentation strategy in which the target region is divided  
79 into two corresponding eddies. Otherwise, the merging and splitting processes cannot be determined properly. This  
80 problem was recently solved by the use of segmentation strategies, e.g., the close-distance segmentation strategy [Li  
81 et al., 2014] and the watershed strategy [Li and Sun, 2015]. Because these segmentation strategies can distinguish  
82 closed eddies, they can also potentially reduce the risk of having a missing eddy in the identification process.

83 Second, the merging and splitting processes in the tracking stage should be described in detail. We use a multi-  
84 branch tree model to do so. The eddy  $E_i$  identified at time step  $k$  may arise from more than one eddy at time step  $k-1$ ,  
85 which subsequently merged; and  $E_i$  may become more than one eddy at time step  $k+1$  if it splits. We refer to this  
86 model as the “Genealogical Evolution Model (GEM)” because it is a genealogical tree for recording the whole  
87 evolutionary history of an eddy. The multi-way tree model in computer science can be used to store this type of  
88 structure.

89 Moreover, the GEM also provides a new way to solve the missing eddy problem. Instead of the existing closest eddy  
90 strategy, a temporal track tree with  $N$  look-ahead time steps is used to maintain all possible tracks with the help of  
91 the multi-way tree model. The method can effectively solve the missing eddy problem, regardless of whether the  
92 eddy is splitting or not.

93 In this paper, we introduce the GEM to describe mesoscale eddies in a tracking process with a total number of time  
94 steps  $T$ . The GEM allows the eddy to have multiple eddies as its parents or as its children in a multi-branch model. It  
95 also solves the missing eddy problem by using a new look-ahead method similar to the MHA. Compared with the  
96 time complexity  $O(M^{N+1}T)$  of MHA, the new method is much faster and has much less time complexity  $O$   
97  $(LM(N+1)T)$ , where  $L$  denotes the pixels of target region. Besides, if the GEM was implemented with the computer  
98 codes properly, the output data of GEM also record the dynamic evolution of the eddy in detail and will potentially

99 be useful for other research fields, e.g., the dynamics of cyclones in meteorology. As an example, The GEM is  
100 applied to eddies in the North Pacific Ocean (NPO) only, and we assume the eddies do not cross the equator.

101 The paper is organized as follows. The data and eddy detection methods used in this study are introduced in section  
102 2. Then GEM is introduced in section 3, including similarity vector, look-ahead approach and the worst-case  
103 runtime complexity i.e. time complexity. Results including eddy tracks and examples of merging and splitting  
104 events in a sample area in the North Pacific are shown in section 4. The impacts of data noise and parameters  
105 uncertainties on the results are discussed in section 5. Finally, a summary and conclusions are given in section 6.

106

## 107 **2 Eddy identification**

### 108 **2.1 Input data**

109 The input data consists of the original altimetry field, which can come from satellite observations or numerical  
110 simulations. The altimetry field used in this study is the 20-year (1993-2012) daily SLA data from the merged and  
111 gridded satellite product of Maps of Sea Level Anomaly (MSLA) at  $0.25^\circ \times 0.25^\circ$  resolution in the global ocean  
112 from AVISO (<http://www.aviso.oceanobs.com/>). In this study, we use the “DT14” (delayed-time 2014) altimeter  
113 product [Duacs/AVISO, 2014], which is adequate for direct eddy detection [Capet et al., 2014] though it still has  
114 about 2-3 cm error globally for short temporal scales [Carrere et al., 2016]. A comprehensive discussion of gridded  
115 Aviso products for eddy investigations can be found in Chelton et al. (2011b).

116 We used the original SLA data (“DT14”) without any filtering or smoothing to identify eddies in this study.  
117 However, this does not imply that data smoothing is not needed for the SLA data in related studies (e.g. eddy  
118 detection, eddy tracking). For example, to calculate some eddy parameters (e.g., velocity and vorticity), smoothing  
119 may be required, as pointed out by Chelton et al. (2011b). Moreover, the data errors, even if they are very small,  
120 might affect the eddy detection (see discussion in section 5.1).

### 121 **2.2 Eddy identification**

122 The eddy identification used in this study is similar to those used before [Chelton et al., 2011b; Mason et al., 2014],  
123 to identify eddies from SLA data. The eddies may be identified with multinuclear (two or more SLA extremes in  
124 one eddy) or mononuclear (only one SLA extremum in one eddy). The following mononuclear eddy definition is also  
125 similar to what was used by other authors [Chaigneau et al., 2011; Li et al., 2014; Li and Sun, 2015]. We have  
126 adopted the eddy detection step from Li and Sun (2015), which provides us with the necessary input for the tracking  
127 routines, namely eddy areas and boundaries. Each pixel has eight nearest neighbours. A point within the region is a  
128 local extremum if it has an SLA greater or less than all of its nearest neighbours. We also use such definition of  
129 extremum in our following analysis, in which the extrema are identified by checking each pixel in the map along  
130 with the eight pixels around it. An eddy is defined as a simply-connected set of pixels that satisfies the following  
131 criteria:

- 132 (1) The SLA value of all of the pixels is above (below) a given SLA threshold;  
133 (2) Only *one* SLA extremum exists in the pixel set;  
134 (3) The amplitude of the eddy (the max difference of SLA values) is larger than a critical value (e.g., 1 cm);  
135 (4) The area of the eddy must be large enough for estimating eddy parameters (say >16 pixels).

136 Conditions (3)-(4) provide the lower bounds for eddy size and amplitude. These conditions automatically reduce the  
137 total number of detected eddies. Condition (1) is the same as the first criterion in Chelton et al., (2011b). It is used in  
138 consideration of the 2-3 cm of background SLA error [Carrere et al., 2016]; so, small fluctuations in SLA field  
139 would not be taken as eddies in this study. Condition (3) was generally used previously [Chaigneau et al., 2011;  
140 Chelton et al. 2011]. Condition (4) is more restrictive than the generally used value of eight pixels [e.g., Chelton et  
141 al., 2011; Li et al., 2014]; so, this condition is an add-on, which is potentially useful when deriving eddy parameters  
142 using a nonlinear optimal fitting method [Wang et al., 2015; Yi et al., 2015]. If the eddy area is too small (only a few  
143 pixels), its parameters (e.g. amplitude, area, radius, etc.) are very sensitive to its area (number of pixels). Besides, we  
144 don't put limits on eddy pixel number maximum (e.g., <1000) and eddy size (e.g., <400-1200 km) while such limits  
145 were generally used previously [e.g., Chelton et al. 2011; Mason et al., 2014].

146 The SLA extremum so determined is called eddy center. The set of pixels belonging to an individual eddy is referred  
147 to as the area of the eddy, and the outmost SLA contour is the boundary of the eddy. We use the area and boundary  
148 to calculate the similarity of eddies in section 3.2.

149 Each eddy is identified by the following procedures. First, according to condition (1), we find a simply-connected  
150 region with a given threshold of  $SLA > 3$  cm for cyclonic eddies and  $SLA < -3$  cm for anticyclonic eddies. Second, we  
151 check whether there is at least one extremum in the region. If the eddy is multinuclear, we use a segmentation  
152 method to segment them to satisfy condition (2). Finally, we check whether the region satisfies the eddy conditions  
153 (3) and (4); we remove those weak (amplitude < 1 cm) and small (pixels < 16) eddies.

154

### 155 **2.3 Eddy segmentation for merging and splitting events**

156 Figure 2 illustrates the necessity for eddy segmentation based on the merging process of two eddies. Two different  
157 mononuclear algorithms are used in the upper and lower rows. In the top panels of Figure 2, eddies are identified by  
158 non-segmentation algorithm. Such mononuclear eddies may be very small. The time evolutions from  $t=1$  to  $t=3$   
159 show a decay scenario of two closed eddies C1 and C2. Both their amplitudes and areas become smaller and smaller  
160 with time. Then, a large eddy C3 suddenly appears in the same region without any premonition. It is hard to see  
161 what happened during the time from  $t=1$  to  $t=3$  from the parameters (amplitude and area) of mononuclear eddies  
162 identified by reducing the number of contours of the SLA until there is only one extreme in the contour (Chaigneau  
163 et al., 2011) instead of the segmentation algorithm [Li and Sun, 2015]. In contrast, the bottom panels of Figure 2  
164 show a merging scenario of two closed eddies C1 and C2 using the segmentation algorithm [Li and Sun, 2015].

165 During the time from  $t=1$  to  $t=2$ , both their amplitudes and areas are only marginally changed, while their distance is  
166 continually reduced. Then, a large eddy C3 naturally emerges in the same region, while C1 and C2 disappear. It is  
167 recognized from the eddy data that C3 is the merging result of C1 and C2.

168 Figure 3 illustrates this eddy segmentation strategy. Figure 3a shows two individual but nearby eddies. The pixels  
169 between the two dashed lines are naturally divided by the watershed (For basins, the “watershed” is a ridge between  
170 them, while it is a valley for plateaus). As shown in Fig. 3b, the cross section of the eddy clearly shows that two  
171 closely located pixels  $P_1$  and  $P_2$  on the left and right sides of watershed would slide along the path of steepest descent  
172 in the map of SLA data to different eddy centres. The shape of SLA can provide sufficient information to segment  
173 the multinuclear eddy into mononuclear ones.

174 Herein, we use the Mononuclear Eddy Identification (MEI) of the Universal Splitting Technology for Circulations  
175 (USTC) with watershed segmentation [Li and Sun, 2015] and include in our code the calculation of eddy parameters,  
176 including amplitude, radius, area, and boundary (Fig. 3), which might be potentially used in other studies [Sun et al.,  
177 2014].

178 The output eddy parameters from MEI is then used as input for our novel tracking algorithm GEM. The GEM  
179 mainly represents the logical relationship of eddies, which is less dependent on physical parameters which may  
180 change greatly because of dynamic evolution (e.g., splitting, merging). To this end, the GEM takes the previously  
181 identified eddies by MEI (with area/boundary, see section 2.2) as its input data.

182

### 183 **3 Dynamic tracking**

#### 184 **3.1 Overview of GEM**

185 The GEM is a logical model used for tracking the dynamic evolution of mesoscale eddies in the ocean (Fig. 4). The  
186 model essentially establishes logical relationships of previously identified eddies. The relationships are determined  
187 by two relatively independent steps i.e. the GEM algorithm consists of two parts (see Fig.4 for details): first,  
188 measuring the “map link” between two time steps and then connecting all time steps to the “track tree”.

189 The first part of GEM is “map link” which uses as input eddy data obtained in the prior eddy identification step  
190 (area/boundary, see section 2.2) to establish the link of an eddy from one temporal snapshot to the next, namely  
191 living, missing, death, birth, and the associated dynamical processes of merging and splitting. In this part of the  
192 work flow, we use a 2-D vector rather than a passive scalar to measure the similarity between eddies  $E_1$  and  $E_2$  on  
193 two neighboring days (Figs. 5 and 6, see section 3.2.1 for details). We then use a relatively complex look-ahead  
194 procedure to solve the missing eddy problem (section 3.2.2). This new look-ahead approach has a duration of  $N$  days  
195 (Fig. 7). Finally, the links of the eddies in different snapshots are saved (see section 3.2.2 for details).

196 The second part is “track tree”, which uses the outputs from “map link” (i.e., eddy links), as its input (Fig. 4). It  
197 connects the eddy links from branches to a tree with the genealogical model (Fig. 8) using two sub procedures:

198 “eddy branch” and “eddy tree”. In the “eddy branch” part, we use *parent* and *child* to define the eddy relationship  
 199 and define all possible types of eddy states: birth, death, living, missing, merging and splitting (Fig. 8a).  
 200 Consequently, we identify different roles in the eddy branches (see section 3.3.1 for details). Finally, in the “eddy  
 201 tree” procedure, we connect the branches based on their roles (parent, child, and grandchild, etc.) in the genealogical  
 202 tree (Fig. 8b). The output of GEM includes eddy tracks and the records of eddy relationships (see section 3.3.2 for  
 203 details).

204 In short, the GEM uses previously identified eddies and/or their links to make dynamic tracks via a genealogical tree  
 205 model. In addition to eddy domain and boundary, it needs two parameters as input, the critical value of area ratio  $r_c$   
 206 and  $N$ . See section 5.2 for discussion on the impacts of these parameter choices.

## 207 3.2 Map link

208 To establish the relationships between the previously identified eddies, the first part of GEM used evaluates the  
 209 similarity of these eddies which is defined here based on the overlap of the domain of an eddy in two consecutive  
 210 time steps. It begins with defining similarity based on the overlapping area of eddies in consecutive time steps.  
 211 Subsequently, the overlapping area which is closest to the one of the original eddy is defined to be the successor of  
 212 the original eddy (if the threshold is met).

### 213 3.2.1 Eddy similarity

214 At first, the eddy similarity is calculated with an example (Fig. 5a) before proceeding to the mathematical  
 215 expressions. There were three eddies A1, A2 and B1 detected on March 28, 1997. In Figure 5b, there were four  
 216 eddies, A1, A2, B1, and B2 on March 29, 1997. We overlapped the eddy domains into a single map (Fig. 5c). Then,  
 217 we used the intersection of eddy domains on different days to calculate the similarity. For eddies A1 and A2, the  
 218 intersections were very close to their respective domains on March 28 and 29. For eddy B1, the intersection was  
 219 close to the area on the second day, but it was only part of that on the first day. Consequently, eddies A1 and A2 had  
 220 full similarity on these days, while eddies B1 and B2 only had partial similarity on these days.

221 To estimate the above similarity, let us describe it in a mathematically logical way. As shown in Figure 6a, there is  
 222 an eddy ( $E_1$ ) that is identified by the thick contour of Boundary 1 in the rectangular comparison region (not shown in  
 223 figure) on day 0, and there are three eddies ( $E_2$ ,  $E_3$  and  $E_4$ ) that are identified in the same region on day 1. This  
 224 comparison region, which is centered at the eddy center of  $E_1$ , moves in time with the target eddy ( $E_1$ ). To determine  
 225 the similarities between  $E_1$  on day 0 and  $E_2$  to  $E_4$  on day 1, we intersect the domains of day 0 and day 1. For example,  
 226 to determine the similarity between  $E_1$  and  $E_2$ , we count the overlap area  $S_{12}$  (defined as the intersection of Boundary  
 227 1 and Boundary 2) between  $E_1$  (area  $S_1$ ) and  $E_2$  (area  $S_2$ ), and then we calculate the following ratios:

$$228 \quad r_1 = S_{12} / S_1, \quad (1a)$$

$$229 \quad r_2 = S_{12} / S_2. \quad (1b)$$

230 Clearly, the values of  $r_1$  and  $r_2$  are within  $[0, 1]$ . The larger  $r_1$  and  $r_2$  are, the larger possibility that  $E_2$  has to be the  
231 snapshot of  $E_1$  on day 1. Eddy movement speeds are generally less than 0.1 m/s, which implies that an eddy can only  
232 move one grid box ( $0.25^\circ$ ) in 3-4 days. Thus, the overlap on different subsequent days of the same eddy area should  
233 be large enough. This is one of the parameters to set. When we applied GEM to track eddies in the Northern Pacific  
234 Ocean, we choose  $r_c=2/3$ , and the choice of  $r_c$  is comprehensively addressed in section 5.2.

235 Using the vector  $(r_1, r_2)$  and the critical value  $r_c$ , we define four different types of similarity between two eddies (Fig.  
236 6b). From low to high, they are as follows: Type 0 (T0:  $r_1 < r_c$  and  $r_2 < r_c$ ), where  $E_1$  and  $E_2$  are unrelated; Type 1 (T1:  
237  $r_1 > r_c$  and  $r_2 < r_c$ ), where  $E_1$  on day 0 is part of  $E_2$  on day 1 ( $E_1$  enlarging or merging); Type 2 (T2:  $r_1 < r_c$  and  $r_2 > r_c$ ),  
238 where  $E_2$  on day 1 is part of  $E_1$  on day 0 ( $E_1$  decaying or splitting); and Type 3 (T3:  $r_1 > r_c$  and  $r_2 > r_c$ ), where  $E_1$  and  
239  $E_2$  are the same eddy at different locations on different days ( $E_1$  living and moving). The last type (T3, living) is  
240 prescribed in cases when the center of  $E_1$  propagates less than a pixel toward that of  $E_2$ , because the eddy movement  
241 speed is physically less than one grid ( $0.25^\circ$ ) per day. For example, eddy B1 on March 29, 1997 in Figure 5b is  
242 simply assigned to T3 (living) even though  $r_1 < r_c$ . Eventually, we obtain the relationships between  $E_1$  and  $E_3$  or  $E_4$   
243 (Fig. 6a). Because the present method uses a vector to express eddy similarity, we call it the similarity vector. This is  
244 an alternative to scalar similarity parameters [e.g., Ienna et al., 2014; Mason et al., 2014].

245 For example, as shown in Figure 6a, the high similarity between  $E_1$  and  $E_2$  over a critical value  $r_c$  (marked as T3  
246 (living) in Fig. 6b) suggests an evolution from  $E_1$  to  $E_2$ . This is similar for eddies  $E_1$  and  $E_3$ , but with a different  
247 splitting relationship (marked as T2 (splitting) in Fig. 6b). The relationship between eddies  $E_1$  and  $E_4$  is designated  
248 as “unrelated” because of the overlap in their areas is small or zero. In other words, their overlap rates are below the  
249 critical value  $r_c$  (marked as T0 in Fig. 6).

250 In previous eddy tracking studies, simple methods were used for weekly SLA data (delayed-time 2010), e.g., the  
251 closest distance between eddies [Chelton et al., 2011b; Yi et al., 2015], the closest angle between eddies [Zhang et  
252 al., 2014] and the dimensionless similarity scalar [Chaigneau et al., 2008; Mason et al., 2014]. There is always a risk  
253 of eddy jumping (from one track to another) in these methods, except for that of Pegliasco et al. (2015), who used  
254 intersections of eddy boundaries to find the continuing eddy. Compared to the previous tracking methods, we use a  
255 more robust technique to assess the relationship of eddies in subsequent time steps by using the overlap of their  
256 areas. In addition, we do not simply assign the continuing eddy using the similarity vector for the two adjacent days;  
257 rather, we try to solve the temporary missing eddy problem by looking ahead a few days.

### 258 3.2.2 Eddy Look-ahead

259 In contrast to the procedure used in Chelton et al. (2011b), we use a relatively complex look-ahead procedure. An  
260 example for a given eddy are shown in Figure 7a. In the upper row, both  $E_{c1}$  and  $E_{c2}$  take the same eddy  $E_{c3}$  as  
261 their subsequent T1 type of eddy, which is a merging event (e.g., eddies C1 and C2 in Fig. 1). Since a T1 (merging)  
262 eddy has  $r_2 < r_c$  (intersection only takes a part of the eddy  $E_{c3}$  on day 1), two or more eddies (e.g.,  $E_{c1}$  and  $E_{c2}$ ) on  
263 day 0 could identify the same eddy ( $E_{c3}$ ) as T1 eddy simultaneously on day 1. In the middle row, eddy  $E_1$  has two  
264 T2 (splitting) type of eddies ( $E_{c2}$ ,  $E_{c3}$ ) at the same time; this is a splitting event (e.g., eddies B1 and B2 in Fig. 5).



265 In the lower row, eddy E1 has T2 (splitting) and T3 (living) types of eddies (respectively Ec2, Ec3) at the same time.  
266 Although there may be many possibilities for any given eddy, there is at most one eddy that can be marked as a T1  
267 (merging) or T3 (living) eddy on the following day (as  $r_l > r_c = 2/3$  holds).

268 This new look-ahead approach with  $N=2$  is shown in Figure 7b. After finishing the calculation of the following  
269 eddies on day 1, we continue to calculate eddies on the following days. At this preparation stage, it is similar to the  
270 MHA method with important modifications [Faghmous et al., 2013]. What makes this look-ahead procedure novel  
271 and efficient is that we use two simple rules to directly choose only one day's result for the following eddies. Thus,  
272 the procedure becomes linear without iteration, and it is much faster than the MHA, as discussed in the subsection  
273 on the time complexity (section 3.4).

274 The two selection rules are: 1) the most similar, and 2) the earliest day. Rule 1 has priority. We first choose the most  
275 similar eddy as the potential successor of Ed1 according to their types. According to Figure 6b, T2 (splitting) type  
276 eddy covers only part of the original eddy while T1 (merging) eddy covers most part of the original eddy. The  
277 similarity from low to high is  $T2 < T1 < T3$ . For example, if there is only one T3 (living) eddy in these days, we  
278 choose it as the potential one. However, if there is more than one day with the same type of eddies, we need an  
279 additional rule: the earliest day. For example, in the upper row of Figure 7b, there is one T3 (living) eddy on day 1  
280 and one T3 (living) eddy on day 2, and there are two T2 (splitting) eddies on day 3. In this case, we choose day 1 as  
281 the following day and the T3 (living) eddy as the following Ed1. In the middle and the lower rows, we choose day 2  
282 and day 3 as the following days and the corresponding T3 (living) eddies as the following Ed2, Ed3 respectively.

283

### 284 3.3 Track tree

#### 285 3.3.1 Eddy branch

286 After having determined the next subsequent days and the relationship types between eddies based on the above  
287 process, we can now establish the branches of an eddy from one day to the next. Eddy branch describes the  
288 relationship between two eddies at two different time steps. To describe the GEM more precisely, we use *parent* and  
289 *child* to identify the different roles that the eddy plays in eddy branches. There are three types of logical  
290 relationships used in GEM, as shown in Figure 8a.

291 The upper row shows a successor relationship: an eddy P on day 1 has only one successor (eddy P itself) on day 2.  
292 In this case, eddy P is allowed to be missing during day 1 and day 2. Additionally, eddy P will be recorded as death  
293 (black circle), if no successor eddy is found after  $N$  days.

294 In the middle row, two (or more) eddies merge into one. The first type includes principal and subordinate merging.  
295 A principal eddy  $P_1$  and a subordinate eddy  $P_2$  on day 1 merge into a larger eddy  $P_1$  on day 2, whereas  $P_2$  is recorded  
296 as death. This occurs when a large eddy meets and merges with a small eddy (e.g., C1 and C2 in Fig. 1). The  
297 anticyclonic eddies A1 and A2 in Fig. 11 also experience a similar process (see section 4.2 for details). The second

298 type is coordinated merging. Two (or more) parent eddies  $P_1$  and  $P_2$  merge to produce a new child eddy  $C$ , and all of  
299 the parent eddies are recorded as death. This is because the similarity is not sufficiently high for either eddy to which  
300 the record of eddy  $C$  should be appended. There might be another choice by keeping parent eddies  $P_1$  and  $P_2$  alive  
301 and appending the record of eddy  $C$  to both eddies. This choice artificially increases lifetimes of eddy  $P_1$  and  $P_2$  and  
302 leads to other tracking problems; so, we abandon it.

303 In the lower row, a parent eddy splits into several child eddies. The first type is principal and subordinate splitting. A  
304 parent eddy  $P$  splits into a relatively large eddy  $P$  (itself, i.e. the similarity type is T3 between the two eddies) and a  
305 relatively small child eddy  $C$  (i.e. the similarity type between parent eddy  $P$  and child eddy  $C$  is a splitting  
306 relationship T2), which is recorded as birth. The second type is coordinated splitting. Two (or more) child eddies are  
307 born from the parent eddy  $P$ , which is then recorded as death. This occurs when all the similarity types between  
308 child eddies and parent eddy are type 2 (T2).

### 309 3.3.2 Eddy tree

310 Finally, the track tree is recorded by connecting the eddy branches (Fig. 8b). Track tree of an eddy records  
311 information of all the associated eddies (e.g., living, death, birth, merging and splitting, etc.) during its entire life. In  
312 this process, the role that an eddy plays in the track tree is considered. The first generation is the parent eddy (e.g.,  
313  $P_1$ ), the second generation is the child eddy (e.g.,  $C_1$ ) and the third generation is the grandchild eddy (e.g.,  $G_1$ ). The  
314 track tree uses the above eddy branches (Fig. 8a). We connect the branches from one time to another to obtain the  
315 whole eddy track tree.

316 There are two additional notations. First, an eddy emerging from the same family of eddies (e.g., two siblings  $C_2$  and  
317  $C_4$ ) will be recorded as a new family member (e.g., eddy  $C_5$ ). Second, an eddy merging from two different families  
318 of eddies (e.g.,  $C_1$  and  $P_2$ ) will be recorded as a new eddy  $N_1$ .

319 Although the model could have several generations, we only recorded two generations i.e. parent and child in this  
320 study due to the complexity of the output data structure and the time complexity. However, we can indirectly track  
321 other generations using the relationships between them.

## 322 3.4 Time complexity

323 To calculate similarity vectors, we need to overlap two small regions around eddy  $E_1$ . The total number of pixels in  
324 the rectangular comparison region is  $L$ . The time complexity of the similarity vector is  $O(L)$  for each day. If we use  
325  $N$  look-ahead time steps to find the best choice, the time complexity of the branches will be  $O(L(N+1))$  for one  
326 eddy. Because all of the steps are linear without iteration, given the maximum number of eddies in any time frame  
327  $M$ , the number of look-ahead time steps  $N$  and the total number of time steps  $T$ , the total time complexity is  $O$   
328  $(LM(N+1)T)$ . The GEM algorithm can hardly be made any faster. When the number of look-ahead time steps  $N$  is  
329 more than one, the time complexity is much faster than  $O(M^{N+1}T)$  of MHA.

330 For example, both  $L$  and  $M$  are approximately 1000, and  $N=2$  is used in the present study. The MHA method will  
331 require on the order of  $10^2$ - $10^3$  times more computational time than the present method; and the larger the value of  $N$ ,  
332 the more efficient the present method is. The look-ahead time  $N$  may be potentially as large as one week ( $N=6$ ), as  
333 noted in the following discussion. Thus, the present method is especially effective compared to the previously  
334 suggested methods when a long look-ahead time is required for poorly identified eddies.

335

## 336 4 Results

### 337 4.1 Eddy tracks

338 We first apply the MEI to detect the ocean eddies in the North Pacific Ocean (NPO) during 1993-2012. The eddy  
339 centers (SLA extrema of eddy snapshots) on each day are counted on each  $1^\circ \times 1^\circ$  grid. In general, anticyclonic eddies  
340 are significantly more frequent than cyclonic eddies. As shown in Figure 9a, the cyclonic eddies are mainly located  
341 in the western part of the NPO. For example, there are lots of cyclonic eddies east of Japan near the Kuroshio, which  
342 can also be seen from both Figure 1 and the results in section 5.1. In contrast, anticyclonic eddies are mainly located  
343 in the eastern part of the NPO (Fig. 9b). For example, the eddies are mainly anticyclones in the red box, which can  
344 also be seen from the results in section 4.2. In general, the eddies are ubiquitous in Figure 9c (about 50-70 eddies per  
345 year on each  $1^\circ \times 1^\circ$  grid), except that there are several regions where both types of eddies are relatively scarce. One  
346 of them is known as “eddy desert” (black box in Figure 9c) [Chelton et al., 2007]. The other region is the North  
347 Equatorial Current (NEC) (blue box in Figure 9c) [Hu et al., 2015]. Finally, we present in Figure 9d the ratio of  
348 difference of the numbers of cyclonic and anticyclonic eddies to the total number of eddies.

349 We apply the GEM to these eddies detected by MEI with  $r_c=2/3$  and  $N=2$ . In the NPO, there are a total of 60276  
350 eddies with lifetimes longer than 30 days. Among them, 37553 of the eddies are anticyclonic and 22723 are cyclonic.  
351 The tracks of long-lived eddies are plotted in Figure 10. In general, they are similar to those shown in previous  
352 studies [Chelton et al., 2011b]. There are 7290 anticyclonic and 3627 cyclonic eddies with lifetimes longer than 100  
353 days (Fig. 10a), and the ratio of anticyclonic to cyclonic eddies is approximately 2. The ratio is larger for eddy  
354 lifetimes greater than 400 days, which was also noted in previous studies [Chelton et al., 2011b; Xu et al., 2011].  
355 Each track is very smooth because we require that the snapshots of eddies on different days overlap one another. We  
356 have done a visual evaluation of many long-lifetime eddy trajectories and the quality of the tracking results is  
357 reasonable. We will take the long-lived C1 in Figure 10b as an example.

358 Eddy C1 was first detected as an eddy initiated on September 14, 1995, with an extremum at  $163.5^\circ\text{W}$ ,  $10.5^\circ\text{N}$ . It  
359 then travelled to the northwest and disappeared at  $151.25^\circ\text{W}$ ,  $20.5^\circ\text{N}$  on March 11, 1997. Its trajectory is the longest  
360 that we have detected in the NPO (Fig. 10b). The trajectory is smooth, except for a sudden jump from  $167.5^\circ\text{E}$  to  
361  $166.75^\circ\text{E}$  (Fig. 10c) on July 31, 1996. The GEM algorithm did very well at whether we should connect the  
362 trajectories from before July 30, 1996 with that after July 31, 1996, into a single trajectory.

363 To clarify this, we plot the two SLA fields in Figure 10d. The SLA field on July 30, 1996 is plotted as contours. The  
364 eddy center is marked by a black cross at 167.5°E, 16.5°N. In contrast, the SLA field on July 31, 1996 is plotted in  
365 shading. The eddy center is marked by a red cross at 166.75°E, 17.25°N. The distance between the eddy extrema was  
366 larger than 100 km within a day. Although that distance is far beyond the criterion applied in standard eddy tracking  
367 routines [Mason et al., 2014; Yi et al., 2015], we can see from the SLA fields that they both indicated the same eddy,  
368 and that it was consistent with our approach to connect the trajectories into a single trajectory.

369 There may be no associated eddy can be identified at the next time step for an eddy at time step  $k$ , and it may be the  
370 result of eddies temporarily “disappearing” for a variety of reasons related to sampling errors and measurement  
371 noise [Chelton et al., 2011b]. The application of similarity vector and look-ahead procedure can effectively  
372 accommodate such problems and allow for the reappearance of temporarily “disappearing” eddy in the tracking  
373 procedure. In turn, the application of similarity vector reduces the usage of the look-ahead procedure. It is clear that  
374 the similarity expressed as a vector is better than that as scalar using simple distance.

## 375 4.2 Eddy merging and splitting

376 The trajectories provide evidence of dynamic evolution. The time evolution of a couple of anticyclonic eddies is  
377 depicted in Figure 11a, which implies a merging process occurring in the red boxes in Fig. 9. As shown in Figure  
378 11a, eddy A1 had a westward movement with a speed of 2.6 cm/s, and eddy A2 lingered near 133°W. Then, both  
379 eddies merged into one large eddy on April 23, 1997. That evolutionary process is clearly shown by the SLA fields  
380 (Figs. 11c-j). In Figure 11c, there were two anticyclonic eddies, A1 and A2, located at 132°W, 28.5°N. Eddy A1  
381 moved from east to west with a nearly constant speed of 2.6 cm/s, whereas eddy A2 had negligible zonal motion.  
382 They then rotated clockwise about each other with an average angular velocity of  $6 \times 10^{-7} \text{ s}^{-1}$ , as denoted by the blue  
383 arrows. Finally, they merged into the new large eddy A2 (see animation in supplement).

384 The SLA field shows that an eddy splitting process also occurred in the box the same time. The time evolutions of  
385 anticyclonic eddies B1, B2 and B3 are depicted in Figure 11b. At first, eddy B1 had a fast westward speed of 10.4  
386 cm/s. It then split into two eddies (B1 and B2) on March 29, 1997 (Fig. 6). Eddy B1 traveled at its original speed  
387 whereas eddy B2 lingered at its origin. Then, eddy B3 emerged at a location between B1 and B2 on April 9, 1997,  
388 which slowed down the speed of B1 to approximately 3.5 cm/s. After that, eddies B2 and B3 merged into a new  
389 eddy B3 on April 19, 1997. In fact, similar to eddies A1 and A2, eddies B1 and B2 eventually merged into a new  
390 eddy on May 20, 1997 (not shown). The SLA maps in Figures 11c-j show more details that were not recorded by the  
391 eddy tracking data. Note that eddy B2 had a very short lifetime of 20 days but a complex dynamic process. If only  
392 long-term eddies (lifetime > 30 days) were saved, the corresponding evolutionary process might not be recorded  
393 properly.

394 It is expected that a pair of cyclonic eddies will have a counter-clockwise rotation in the Northern Hemisphere,  
395 which is known as the Fujiwhara effect for atmospheric cyclones [Fujiwhara, 1921]. When two cyclones are close  
396 enough, they will begin to orbit cyclonically (counter-clockwise in the Northern Hemisphere). Because the above-

397 mentioned eddies are anticyclonic, they have opposing directions of rotation, which appear as two point vortices  
398 moving in circular paths about the center of vorticity in classical fluid dynamics [Batchelor, 1967].

### 399 **4.3 Census of merging and splitting events**

400 To illuminate how often the merging and splitting processes occurred, we counted the total number of merging and  
401 splitting events on each  $1^\circ \times 1^\circ$  grid each year. The merging and splitting events were homogeneously distributed in  
402 the oceans, but in general were very few times each year per  $1^\circ \times 1^\circ$  grid element. The merging frequencies for  
403 cyclonic eddies and anticyclonic eddies are shown in Figure 12, which are similar to their splitting frequencies (not  
404 shown). The distribution pattern of merging frequencies for cyclonic eddies in Figure 12a, is very similar to that of  
405 cyclonic eddy centers in Figure 9a. In contrast, the merging frequency for anticyclonic eddies was larger along the  
406 west coast (Fig. 12b), whereas the anticyclonic eddy centers were located mainly in the east (Fig. 9b). Although  
407 merging and splitting events may occur anywhere in the ocean there is spatial variation in the number of events (Fig  
408 12c, d)

409 The first type of special region is the western boundary. It is known that the western boundary is a sink of eddy  
410 energy caused by the interaction with the bottom and lateral topography [Zhai et al., 2010]. It is also known as a  
411 “graveyard” for westward-propagating ocean eddies [Zhai et al., 2010; Chelton et al., 2011b]. The second type of  
412 special region is located in strong currents, including the Kuroshio Current, and the NEC [Hu et al., 2015]. Among  
413 those currents, the eddies in the NEC had the highest frequency of merging and splitting events, which was not  
414 noted in previous studies. The third type of special region is located in the northeast Pacific, which is also known as  
415 an “eddy desert” [Chelton et al., 2007]. The fourth type of special region is located in enclosed marginal seas,  
416 especially the Bering Sea.

417 By comparing Figure 12 with Figure 10, we can see that the regions with high frequencies of merging and splitting  
418 events have relatively few eddy tracks, especially in the NEC (blue box in Figure 9c) and in the “eddy desert” (black  
419 box in Figure 9c) in the northeast Pacific. The existence of “eddy desert” may be due to the fact that the eddy was  
420 too small to be detected or the fact that the eddy lifetime was too short [Chelton et al., 2011b]. However, Figures 9  
421 and 12 suggest that merging and splitting events may be a major contributor to the “eddy desert”.

422 We also calculate the average dynamic (merging and splitting) events per eddy as a function of lifetime (Figure 13).  
423 The results are similar regardless eddy polarizations and dynamic types. The merging and splitting events are  
424 approximately linear increase with eddy lifetime. However, the anticyclonic eddies seem more vigorous in ocean  
425 dynamics than cyclonic eddies.

426

## 427 5 Discussion

### 428 5.1 Data noise

429 Although “the Aviso product DT14” is much better than previous products, there are still some notable errors,  
430 especially for short temporal scales of less than two months [Carrere et al., 2016]. It was reported that there are  
431 along-track SLA errors of about 2-3 cm globally and of more than 3 cm at high latitudes and in shallow waters.

432 To reduce the noise in SLA data, one may use the Gaussian structure filter [Chelton et al., 2011b; Mason et al.,  
433 2014], Hanning filters [Penven et al., 2005], or Lanczos filter [Chaigneau et al., 2008]. As certain parameters need to  
434 be chosen in these filters, the filtered results depend much on these parameters [see Fig. A1 in Chelton et al., 2011b].  
435 As sensitivity test we apply a simple five-point quadratic smoothing to the SLA data. The filtered data are then  
436 piecewise  $C^2$ -smoothed by a quadratic function, which satisfies the potential requirements for calculating vorticity  
437 (second derivative of SLA) from SLA data.

438 Figure 14 shows the non-smoothed and smoothed SLA data from January 1, 1993 to January 4, 1993. The smoothed  
439 SLA maps are very close to the non-smoothed SLA maps. And the values at the SLA extrema (not shown) are close  
440 to their original values. This implies that the noise in the DT14 data is sufficiently small for our purpose.

441 However, the noise cannot be neglected, even when they are small. They might induce additional SLA extrema (see  
442 the definition of extremum in section 2.2), which eventually affect eddy detection, e.g., the additional extremum on  
443 January 2, 1993 in box A and the additional extremum on January 3, 1993 in box B (Figure 14). These additional  
444 extrema existed only for a very short period (one or two days). But they can induce additional merging and splitting  
445 events, which may cause eddies to unexpectedly terminate [Chelton et al., 2011b]. The ambiguity of the eddy  
446 identification procedure, which may be caused by sampling errors and measurement noise in the input SLA data,  
447 strongly suggest the application of a look-ahead approach.

### 448 5.2 Impact of variations of parameters

449 To discuss the impact of the GEM critical value  $r_c$  and look-ahead time  $N$ , we carry out a sensitivity study in the  
450 north Pacific from year 1993 to 2012. The number of eddies with lifetimes  $> 30$  days is counted for different  $r_c$  and  
451  $N$ , as shown in Figure 15a. Note that the results are very similar, except for  $N=0$  (i.e., without any look-ahead). It is  
452 from the above discussion that we see look-ahead is necessary when there are extrema due to small noise in the data.  
453 The number of eddies does not change substantially with  $r_c$  for any  $N>1$ , when  $r_c$  is within 0.5 to 0.8 (e.g. 63469  
454 eddies were identified with  $N=2$ ,  $r_c=0.5$  and the identified eddies number was 63630 with  $N=4$ ,  $r_c=0.8$ ). Meanwhile,  
455 the numbers of merging and splitting events are also counted for different  $r_c$  and  $N$ , as shown in Figure 15b. In  
456 general, the splitting events occurs slightly more frequently than the merging events (e.g. 151220 splitting events  
457 and 150612 merging events for  $N=2$ ,  $r_c=0.5$ ). Note also that the results are very similar, except for  $N=0$ . The  
458 numbers of merging and splitting events seem to converge for  $r_c > 0.5$  as  $N$  increases. For each  $N>0$ , the numbers of  
459 merging and splitting events reach a maximum at  $r_c=0.6$ . A relatively loose similarity condition ( $r_c < 0.5$ ) will lead to

460 a risk of eddy jumping from one track to another, which consequently reduces both total eddy number and dynamic  
461 events. On the other hand, a relatively strict similarity condition ( $r_c > 0.9$ ) will lead to a risk of missing eddies, which  
462 may also reduce both total eddy numbers and dynamic events.

463 In general, one would like the tracking results to be insensitive to the choice of these parameters. From Figure 15,  
464 we can observe that  $0.5 < r_c < 0.8$  appears to be a choice with relatively robust results. The optimal value for  $r_c$  might  
465 be 0.6-0.7, which is reasonable. In one hand, we first require that  $r_c > 0.5$ . On the other hand, we know there is area  
466 error in calculation ( $\sim 10\%$ ) since only eddy grids are taken into consider. This is also the reason why we need  $r_c$   
467  $< 0.9$  or even smaller. So the optimal value should be within 0.5-0.9, and  $\sim 0.7$  is just in this middle. We also find that  
468 the look-ahead time  $N$  should be larger than 0; otherwise, the risks of eddy jumping and eddy missing are too great.  
469 The look-ahead approach effectively reduces such risks. For example,  $N=1$  and  $N=2$  have 95.5% and 98% of the  
470 total eddies for  $N=4$ , respectively. To reduce the missing eddies to 1%, the look-ahead time might be greater than six  
471 days. This is also the physical requirement of the representative period of the merged SLA data [Chelton et al.,  
472 2011b]. Although  $N=4$  might be better,  $N=2$  produced a very similar result ( $\sim 2\%$  bias to  $N=4$ ) and with a  
473 significantly lower computational cost. Our present parameters are reasonable considering of computational cost.

474 It should be pointed out that GEM is relatively independent to MEI, but the ratios  $r_1$ ,  $r_2$  and  $r_c$  might be sensitive to  
475 the method used in identification. We noted that GEM based on Okubo–Weiss (O–W) parameter identification is  
476 much sensitive to the critical value  $r_c$  than SLA based one, since O–W based eddies are much smaller and more  
477 possible to be unreal [Chaigneau et al., 2008]. Besides,  $r_c$  may not be independent with  $N$ , and the present  $r_c$  should  
478 only be valid for small time steps. If the time step is too large, the distance of eddy motion may be too far. And eddy  
479 snapshots can't overlap with each other. This constrain for time step is something like the Courant–Friedrichs–Lewy  
480 (CFL) condition (for time step) in computer fluid dynamics. In general, we think any tracking method should have  
481 this time-step limitation (depending on eddy size/propagation speed), if one don't want to mix one signal with  
482 another.

483 Finally, as noted in section 4.2, there are short-term eddies (lifetime  $< 30$  days), which might experience complex  
484 evolution process. If only long-term eddies (lifetime  $> 30$  days) were saved, the corresponding evolution process  
485 might not be recorded properly. This should be noted in further applications on eddy dynamics with satellite  
486 altimetry data.

### 487 **5.3 Impact of eddy boundary**

488 It is difficult to directly compare the influences of eddy boundary due to parameter choice in eddy identification. We  
489 can, however, estimate the influence of the eddy boundary using an indirect way. Because the eddy center is  
490 relatively robust, different identification methods mainly give different eddy boundaries. Consequently, the eddy  
491 area  $S$  is most sensitive to such an eddy area. However, the area ratio reduces the sensitivity to the eddy area  $S$   
492 because both the overlap area  $S_{I2}$  and the eddy area  $S$  change synchronously. Moreover, our tracking results  
493 fortunately are not very sensitive to  $r_c$  (or the eddy area  $S$ ), as noted in the above discussion. For example, the

494 present results are based on a very strict identification method. If we modify the threshold of eddy amplitude from 1  
495 cm to 3 cm, the number of identified eddies will decline. Nevertheless, the identification results for the long-lived  
496 eddies appear to be similar (Table 1).

497 However, such sensitive test may be only valid for the comparison of different parameter values in a same  
498 identification method. It can't be simply extended to the comparison of eddies identified by different methods, since  
499 the eddy detection algorithms differ a lot from each other. In general, the automated eddy detection algorithms are  
500 categorized into three types: 1) physical parameter-based algorithms, e.g., Okubo–Weiss (O–W) parameter [Isern-  
501 Fontanet et al., 2003; Chaigneau et al., 2008]; 2) flow geometry-based algorithms [Chaigneau et al., 2011; Chelton  
502 et al., 2011b; Wang et al., 2015]; and 3) hybrid methods, which involve physical parameters and flow geometry  
503 characteristics [Nencioli et al., 2010; Xiu et al., 2010; Dong et al., 2011; Yi et al., 2015]. For example, Yi et al.  
504 (2015) used the O–W parameter to identify eddy kernels and SLA contour geometries to identify eddy boundaries.  
505 So it is difficult to compare the influences of eddy territory by using different identification and tracking algorithms.  
506

#### 507 **5.4 Future research**

508 The GEM is a flexible model that can easily work with other relevant programs, e.g., data filtering and smoothing  
509 algorithms [Chelton et al., 2011b; Ienna et al., 2014; Wang et al., 2014], other hybrid eddy detection algorithms [e.g.,  
510 Yi et al., 2015] and O-W parameter detection [e.g., Petersen et al., 2013], because the GEM only requires a flow  
511 field and previously identified eddies to accomplish dynamic tracking. In addition, the similarity measurement can  
512 be replaced by similar methods [e.g., Pegliasco et al., 2015] when considering more complex conditions.

513 The identified eddies by using other identification algorithm without watershed can also be tracked with the GEM.  
514 In this case, the strong interaction stage of eddies “in conjunction”, which leads to genesis and termination of eddies,  
515 is more likely missed as pointed out in section 2.3. However, the weak interaction stage of eddies (watershed free) in  
516 some far distance could still be recorded, because most of merging/splitting records occurred at the interaction of  
517 two eddies with a certain distance. This weak interaction still can't be recorded by previously interaction-free  
518 tracking algorithm, which records only the isolated tracks. Thus the GEM extends the potential applications of  
519 previously identified eddies.

520 The GEM is a complex model. The output data include eddy tracks, relationships and previously identified eddy  
521 characteristics (e.g., amplitude and radius). These eddy characteristics, which were directly obtained from the  
522 identification process, are useful for censuses [Chelton et al., 2011b]. However, they may not be sufficiently  
523 accurate for some applications. For example, eddy area was required in our recent studies on typhoons and oceanic  
524 eddy interactions [Sun et al., 2010, 2012, 2014]. Besides, some physical quantity (circulation, angular momentum,  
525 energy) are required to be accurately calculated in the investigation of eddy dynamics process. A better way to  
526 obtain these characteristics might be to use a nonlinear fitting of the flow field [Wang et al., 2015; Yi et al., 2015]  
527 with appropriate models [e.g., Sun, 2011; Zhang et al., 2013] other than simply estimated from identification.



528 Another future research direction may involve comparing different tracking datasets. Because there are several  
529 tracking datasets produced by various methods, it is useful to inter-compare them. This may improve both the  
530 tracking methods and the available datasets for further studies.

531 The GEM can be easily applied to larger datasets, even to 3-D numerical simulation outputs [Petersen et al., 2013;  
532 Woodring et al., 2016], because its computational time increases only linearly as a function of the size of the dataset.  
533 The computation of the 20-year daily global SLA data only required a few hours on a personal computer. In a  
534 personal computer with CPU of i7-6700k and 4.00 GHz, it takes about 15 minutes to identify snapshots of eddies,  
535 about 20 minutes to establish similarity, and about 10 minutes to track eddies in the North Pacific Ocean (NPO) with  
536  $0.25^\circ \times 0.25^\circ$  resolution of 20-year daily “DT14” data. Such a model can be used to analyze numerical simulation  
537 outputs.

538 The GEM opens a window to investigate eddy dynamics [Wang et al., 2015] and other applications [Sun et al., 2014]  
539 on those problems, e.g. (i) the strong eddy interaction which leads to genesis and termination of eddies (ii) the weak  
540 eddy interaction which associates with merging/splitting events (iii) the weak eddy interaction which modulates the  
541 eddy track and motion. As illuminated in Figure 11, the dynamic evolution of eddies is accompanied by abundant  
542 phenomena that might be identified using the GEM. The present study is only the beginning of such applications.

543

## 544 **6 Conclusions**

545 We have introduced the GEM for the tracking of the dynamic evolution of mesoscale eddies in the ocean. Several  
546 novel approaches (e.g., vector similarity and look-ahead approach) were applied to deal with unsolved problems in  
547 tracking. All of the computational steps in GEM are linear and do not require iteration. Given the grid number of the  
548 target region  $L$ , the maximum number of eddies  $M$ , the number of look-ahead time steps  $N$ , and the total time steps  $T$ ,  
549 the total time complexity is of  $O(LM(N+1)T)$ . We applied the GEM to the eddies in the north Pacific. Eddy tracks  
550 were smooth because we required that the snapshots of eddies on neighboring days overlap one another. Both  
551 merging and splitting rates of eddies were high, especially at the western boundary, in strong currents and in “eddy  
552 deserts”. The GEM is useful not only for satellite-based observational data but also for the output of numerical  
553 simulations. It potentially has many applications for studies of dynamic processes in related fields, e.g., the  
554 dynamics of cyclones in meteorology. The “MEI” and “GEM” computer codes and program manual will be  
555 provided openly at the website [https://www.researchgate.net/profile/Liang\\_Sun20/](https://www.researchgate.net/profile/Liang_Sun20/) after publication of this  
556 paper.

557

558

## 559 **Acknowledgements**

560 We thank the anonymous referees and Dr. John M. Huthnance for their comments and suggestions. We thank the  
561 AVISO for providing the SLA data (<http://www.aviso.oceanobs.com/>). This work was supported by the National  
562 Basic Research Program of China (Nos. 2012CB417402 and 2013CB430303), the National Foundation of Natural  
563 Science (No. 41376017) and the Open Fund of the State Key Laboratory of Satellite Ocean Environment Dynamics  
564 (No. SOED1501).  
565

566 **References**

- 567 Batchelor, G. K. (2000). *An introduction to fluid dynamics*. Cambridge university press, 615pp.
- 568 Bennett, A. F., & White, W. B. (1986). Eddy heat flux in the subtropical North Pacific. *J. Phys. Oceanogr.*, 16(4),  
569 728-740.
- 570 Capet, A., E. Mason, V. Rossi, C. Troupin, Y. Faugère, I. Pujol, and A. Pascual, (2014), Implications of refined  
571 altimetry on estimates of mesoscale activity and eddy-driven offshore transport in the Eastern Boundary Upwelling  
572 Systems, *Geophys. Res. Lett.*, 41, 7602–7610, doi:10.1002/2014GL061770.
- 573 Carrere, L., Faugère, Y., and Ablain, M. (2016). Major improvement of altimetry sea level estimations using  
574 pressure-derived corrections based on ERA-Interim atmospheric reanalysis, *Ocean Sci.*, 12, 825-842,  
575 doi:10.5194/os-12-825-2016.
- 576 Chaigneau, A., Gizolme, A., and Grados, C. (2008). Mesoscale eddies off Peru in altimeter records: identification  
577 algorithms and eddy spatio-temporal patterns. *Progr. Oceanogr.*, 79, 106–119.
- 578 Chaigneau, A., Le Texier, M., Eldin, G., Grados, C., and Pizarro, O. (2011). Vertical structure of mesoscale eddies  
579 in the eastern South Pacific Ocean: A composite analysis from altimetry and Argo profiling floats, *J. Geophys. Res.:  
580 Oceans*, 116. C11025, doi:10.1029/2011JC007134.
- 581 Chelton, D.B., Schlax, M.G. (1996). Global observations of oceanic Rossby waves. *Science* 272, 234–238.
- 582 Chelton, D. B., Schlax, M. G., Samelson, R. M., & de Szoeke, R. A. (2007). Global observations of large oceanic  
583 eddies. *Geophys. Res. Lett.*, 34(15), L15606. doi:10.1029/2007GL030812.
- 584 Chelton, D. B., Gaube, P., Schlax, M. G., Early, J. J., & Samelson, R. M. (2011a). The influence of nonlinear  
585 mesoscale eddies on near-surface oceanic chlorophyll. *Science*, 334(6054), 328-332.
- 586 Chelton, D. B., Schlax, M. G., & Samelson, R. M. (2011b). Global observations of nonlinear mesoscale eddies.  
587 *Progr. Oceanogr.*, 91(2), 167-216.
- 588 Dong, C., Nencioli, F., Liu, Y., & McWilliams, J. C. (2011). An automated approach to detect oceanic eddies from  
589 satellite remotely sensed sea surface temperature data. *Geoscience and Remote Sensing Letters, IEEE*, 8(6), 1055-  
590 1059.
- 591 Dong, C., McWilliams, J. C., Liu, Y., & Chen, D. (2014). Global heat and salt transports by eddy movement. *Nature  
592 communications*, 5:3294, DOI: 10.1038/ncomms4294.
- 593 Duacs/AVISO (2014), A new version of SSALTO/Duacs products available in April 2014. Version 1.1, CNES.  
594 [Available at <http://www.aviso.altimetry.fr/fileadmin/documents/data/duacs/Duacs2014.pdf>].
- 595 Fang, F., and Morrow, R. (2003). Evolution, movement and decay of warm-core Leeuwin Current eddies. *Deep-Sea  
596 Res., Part II* 50, 2245–2261.

597 Fujiwhara, S. (1921). "The natural tendency towards symmetry of motion and its application as a principle in  
598 meteorology". *Q. J. R. Met. S.* 47 (200): 287–293. doi:10.1002/qj.49704720010.

599 Faghmous, J. H., Uluyol, M., Styles, L., Le, M., Mithal, V., Boriah, S., & Kumar, V. (2013). Multiple Hypothesis  
600 Object Tracking For Unsupervised Self-Learning: An Ocean Eddy Tracking Application. In *AAAI*.

601 Hu, D., Wu, L., Cai, W., Gupta, A. S., Ganachaud, A., Qiu, B. ... & Wang, G. (2015). Pacific western boundary  
602 currents and their roles in climate. *Nature*, 522(7556), 299-308.

603 Ienna, F., Jo, Y. H., & Yan, X. H. (2014). A new method for tracking Meddies by satellite altimetry. *Journal of*  
604 *Atmospheric and Oceanic Technology*, 31(6), 1434-1445.

605 Isern-Fontanet, J., García-Ladona, E., & Font, J. (2003). Identification of marine eddies from altimetric maps.  
606 *Journal of Atmospheric and Oceanic Technology*, 20(5), 772-778.

607 Li, Q. Y., Sun, L., Liu, S. S., Xian, T., & Yan, Y. F. (2014). A new mononuclear eddy identification method with  
608 simple splitting strategies. *Remote Sensing Letters*, 5(1), 65-72. doi:10.1080/2150704X.2013.872814.

609 Li, Q. Y., & Sun, L. (2015). Technical Note: Watershed strategy for oceanic mesoscale eddy splitting. *Ocean*  
610 *Science*, 11(2), 269-273. doi: 10.5194/os-11-269-2015.

611 Mason, E., Pascual, A., & McWilliams, J. C. (2014). A new sea surface height–based code for oceanic mesoscale  
612 eddy tracking. *Journal of Atmospheric and Oceanic Technology*, 31(5), 1181-1188.

613 McGillicuddy, D. J. (2011). Eddies masquerade as planetary waves. *science*, 334(6054), 318-319. doi:  
614 10.1126/science.1208892.

615 Nencioli, F., Dong, C., Dickey, T., Washburn, L., & McWilliams, J. C. (2010). A vector geometry-based eddy  
616 detection algorithm and its application to a high-resolution numerical model product and high-frequency radar  
617 surface velocities in the Southern California Bight. *Journal of Atmospheric and Oceanic Technology*, 27(3), 564-579.

618 Penven, P., Echevin, V., Pasapera, J., Colas, F., and Tam, J.: Average circulation, seasonal cycle, and mesoscale  
619 dynamics of the Peru Current System: A modeling approach, *J. Geophys. Res.*, 110, C10021,  
620 doi:10.1029/2005jc002945, 2005.

621 Petersen, M. R., Williams, S. J., Maltrud, M. E., Hecht, M. W., & Hamann, B. (2013). A three-dimensional eddy  
622 census of a high-resolution global ocean simulation. *Journal of Geophysical Research: Oceans*, 118(4), 1759-1774.

623 Pegliasco, C., A. Chaigneau, and R. Morrow, (2015). Main eddy vertical structures observed in the four major  
624 Eastern Boundary Upwelling Systems, *J. Geophys. Res. Oceans*, 120, 6008–6033, doi:10.1002/2015JC010950.

625 Sun L, Yang Y.-J., Xian T., Lu Z. and Fu Y.-F., (2010). Strong enhancement of chlorophyll a concentration by a  
626 weak typhoon, *Mar. Ecol. Prog. Ser.*, 404, 39-50, doi: 10.3354/meps08477.

627 Sun, L. (2011). A typhoon-like vortex solution of incompressible 3D inviscid flow. *Theoretical and Applied*  
628 *Mechanics Letters*, 1(4), 042003.

629 Sun, L., Yang, Y.-J., Xian, T., Wang, Y., and Fu, Y.-F., (2012). Ocean responses to Typhoon Namtheun explored  
630 with Argo floats and multiplatform satellites. *Atmos. Ocean.* 50(sup1), 15-26.

631 Sun, L., Y.-X. Li, Y.-J. Yang, Q. Wu, X.-T. Chen, Q.-Y. Li, Y.-B. Li, & T. Xian (2014). Effects of super typhoons  
632 on cyclonic ocean eddies in the western North Pacific: A satellite data-based evaluation between 2000 and 2008, *J.*  
633 *Geophys. Res. Oceans*, 119(9): 5585–5598, doi:10.1002/2013JC009575.

634 Wang, R., Yang, Z., Liu, L., Deng, J., & Chen, F. (2014). Decoupling noise and features via weighted L1-analysis  
635 compressed sensing. *ACM Transactions on Graphics (TOG)*, 33(2), 1-12.

636 Wang, Z., Li, Q., Sun, L., Li, S., Yang, Y., & Liu, S. (2015). The most typical shape of oceanic mesoscale eddies  
637 from global satellite sea level observations. *Frontiers of Earth Science*, 9(2), 202-208. doi: 10.1007/s11707-014-  
638 0478-z.

639 Woodring, J., Petersen, M., Schmeiber A., Patchett J., Ahrens J., Hagen H., (2016). In Situ Eddy Analysis in a High-  
640 Resolution Ocean Climate Model, *IEEE Transactions on Visualization & Computer Graphics*, 22(1), 857-866,  
641 doi:10.1109/TVCG.2015.2467411

642 Xiu, P., Chai, F., Shi, L., Xue, H., & Chao, Y. (2010). A census of eddy activities in the South China Sea during  
643 1993–2007. *Journal of Geophysical Research: Oceans*, 115(C3). C03012, doi:10.1029/2009JC005657

644 Xu, C., Shang, X. D., & Huang, R. X. (2011). Estimate of eddy energy generation/dissipation rate in the world  
645 ocean from altimetry data. *Ocean Dynamics*, 61(4), 525-541.

646 Yang, G., Wang, F., Li, Y., Lin, P., (2013). Mesoscale eddies in the northwestern subtropical Pacific Ocean:  
647 Statistical characteristics and three-dimensional structures. *Journal of Geophysical Research: Oceans*, 118(4): 1906–  
648 1923.

649 Yi, J., Du, Y., Zhou, C., Liang, F., & Yuan, M. (2015). Automatic Identification of Oceanic Multieddy Structures  
650 From Satellite Altimeter Datasets. *IEEE JSTARS*, 8(4): 1555-1563.

651 Zhai, X., Johnson, H. L., & Marshall, D. P. (2010). Significant sink of ocean-eddy energy near western boundaries.  
652 *Nature Geoscience*, 3(9), 608-612.

653 Zhang, C. H., Xi, X. L., Liu, S. T., et al. (2014). A mesoscale eddy detection method of specific intensity and scale  
654 from SSH image in the South China Sea and the Northwest Pacific. *Science China: Earth Sciences*, 57: 1897–1906,  
655 doi: 10.1007/s11430-014-4839-y.

656 Zhang, Z., Zhang, Y., Wang, W., & Huang, R. X. (2013). Universal structure of mesoscale eddies in the ocean.  
657 *Geophysical Research Letters*, 40(14), 3677-3681. doi: 10.1002/grl.50736.

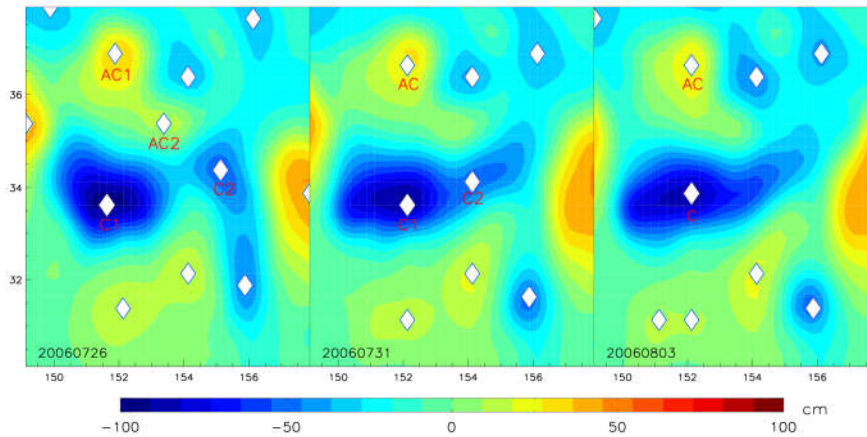
658

659

660 Table 1. The census of long-lived eddies, where “Amp” represents the amplitude threshold used in eddy detection;  
 661 and “C” and “AC,” respectively, represent cyclonic and anticyclonic eddies.

Amp	AC (>100 d)	C (>100 d)	AC (>400 d)	C (>400 d)
1 cm	7290	3627	198	22
3 cm	7118	3550	194	21

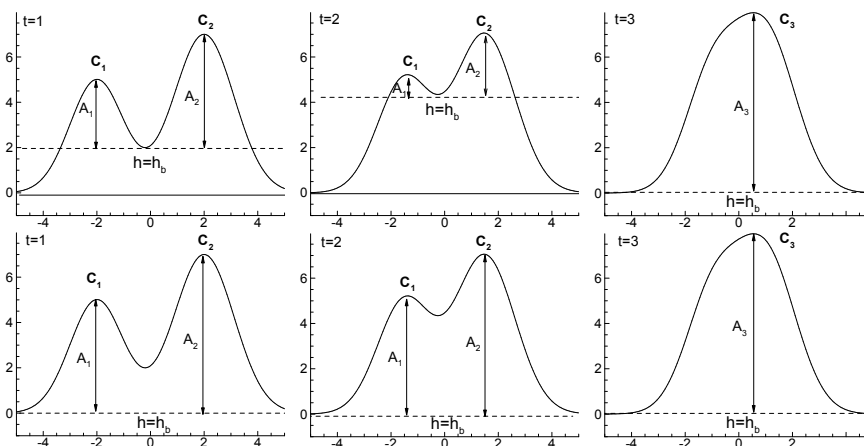
662



663

664 Figure 1. The evolutions of amplitudes and areas of eddies from July 5 to August 3, 2006 (after Li et al. 2014),  
 665 where the background field shows SLA, and white dots mark eddy centers. Two anticyclonic eddies AC1 and  
 666 AC2 merged into a single eddy on July 31, 2006. And, two cyclonic eddies C1 and C2 merged into a single one on  
 667 August 3, 2006.

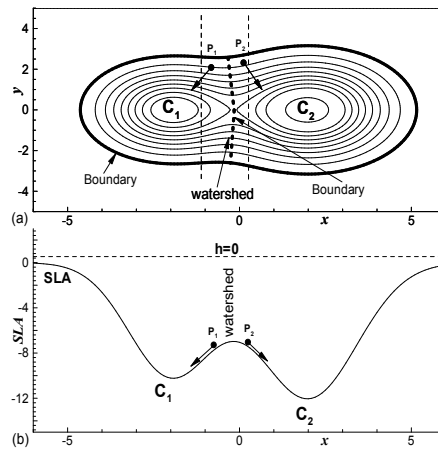
668



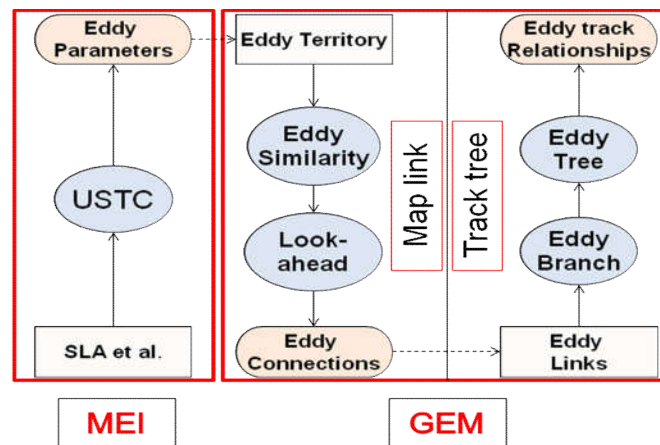
669

670 Figure 2. Top panels: Time evolution of two merging eddies revealed by the mononuclear eddy identification  
 671 without segmentation. Bottom panels: Time evolution of two merging eddies revealed by the mononuclear eddy

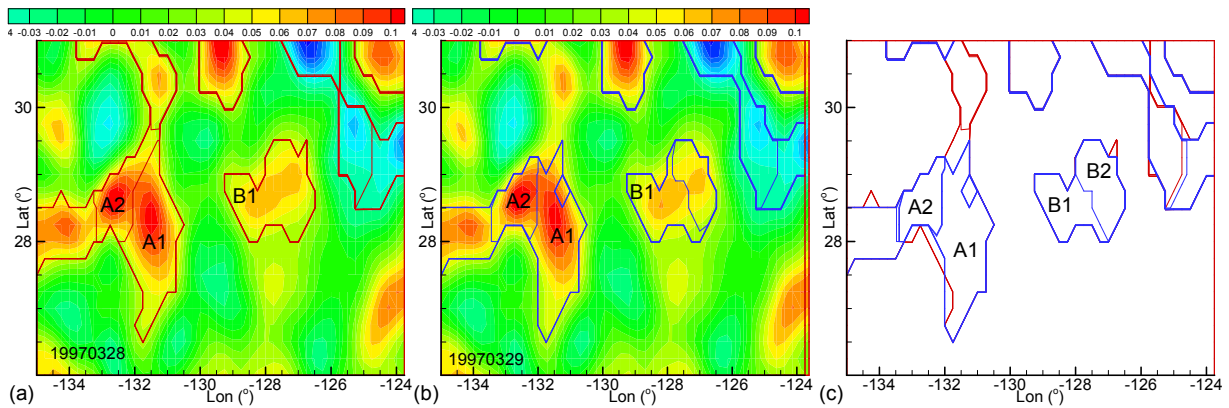
672 identification with segmentation. The  $h$  represents background SLA value,  $A$  represents amplitude of eddy,  
 673 and  $t$  represents the map at different time.



674  
 675 Figure 3. (a) Watershed as the natural division of eddies  $C_1$  and  $C_2$  from top view, where contours represent SLA. (b)  
 676 The particles  $P_1$  and  $P_2$  on the watershed flow downward to the eddy centres  $C_1$  and  $C_2$  from cross-section view.  
 677  
 678 After Li and Sun (2015).



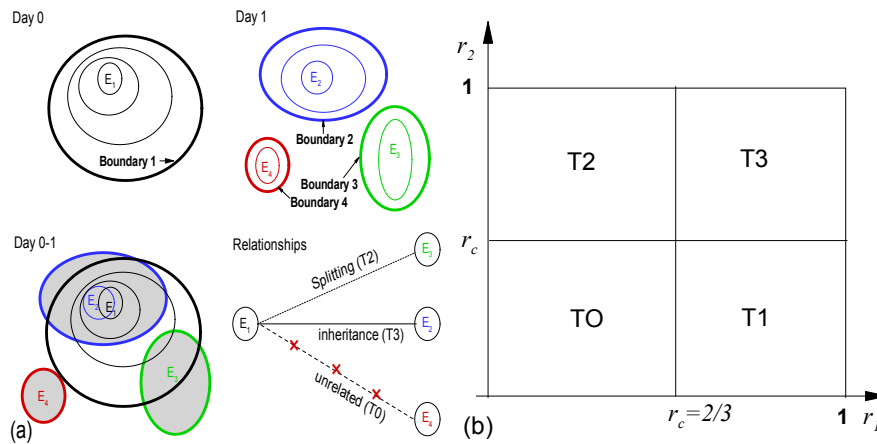
679  
 680 Figure 4. Flow chart of the systems. Mononuclear Eddy Identification (MEI) uses SLA to identify eddies via the  
 681 Universal Splitting Technology for Circulations (USTC) method. The GEM, which has two independent parts of  
 682 “Map link” and “Track tree”, then uses the previously identified eddies for tracking.  
 683  
 684  
 685



686

687 Figure 5. Sketch of eddy overlaps. (a) The SLA map (shading) and the boundary of eddies (red curves) on March 28,  
 688 1997, where A1, A2 and B1 represent identified eddies. (b) The SLA map (shading) and the boundary of eddies (blue  
 689 curves) on March 29, 1997. (c) The intersection of eddy areas by overlap eddy identification maps.

690

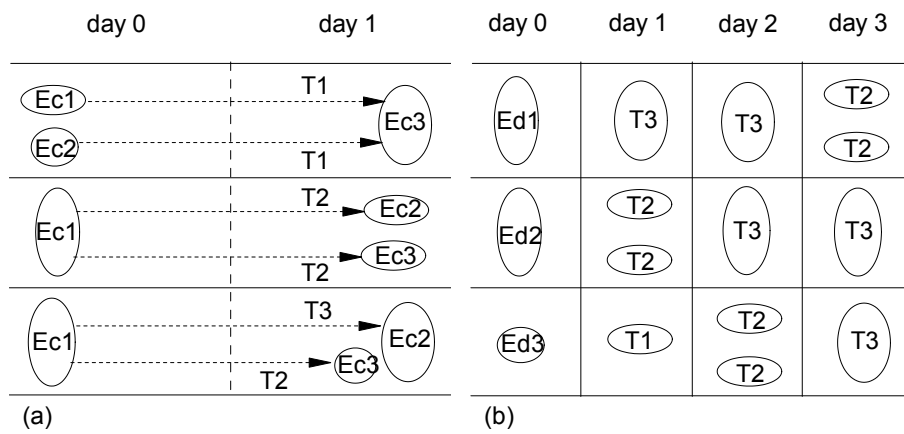


691

692 Figure 6. Sketch of eddy similarities. (a) The sketch of eddy overlaps. Eddy  $E_1$  (black) is the eddy identified on day  
 693 0, where the thin contours represent the eddy parameter (e.g., the SLA value). The thick contour represents the eddy  
 694 boundary. Eddies  $E_2$  (blue),  $E_3$  (green) and  $E_4$  (red) are identified on day 1. We consider the overlay between the two  
 695 eddies on different days to evaluate the similarity between them. (b) There are four similarity types (T0-T3)  
 696 according to the values of  $r_1$ ,  $r_2$  and the critical value  $r_c$ , there is at most one eddy that can be marked as a T1  
 697 (merging) or T3 (living) eddy on the following day.

698





699

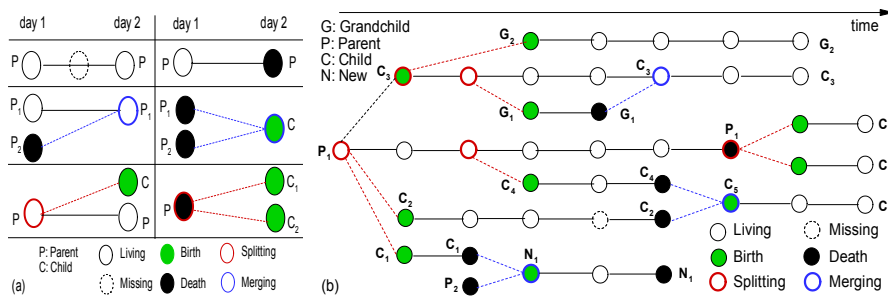
700

701

702

703

Figure 7. (a) Three typical cases of successors (T1, T2 and T3) from one day (day 0) to another (day 1). (b) The eddy at day 0 may have different successors corresponding to different numbers of “look-ahead” days, e.g., Ed1 at day 0 may have a T3 eddy on day 2, and have two T2 eddies on day 3.



704

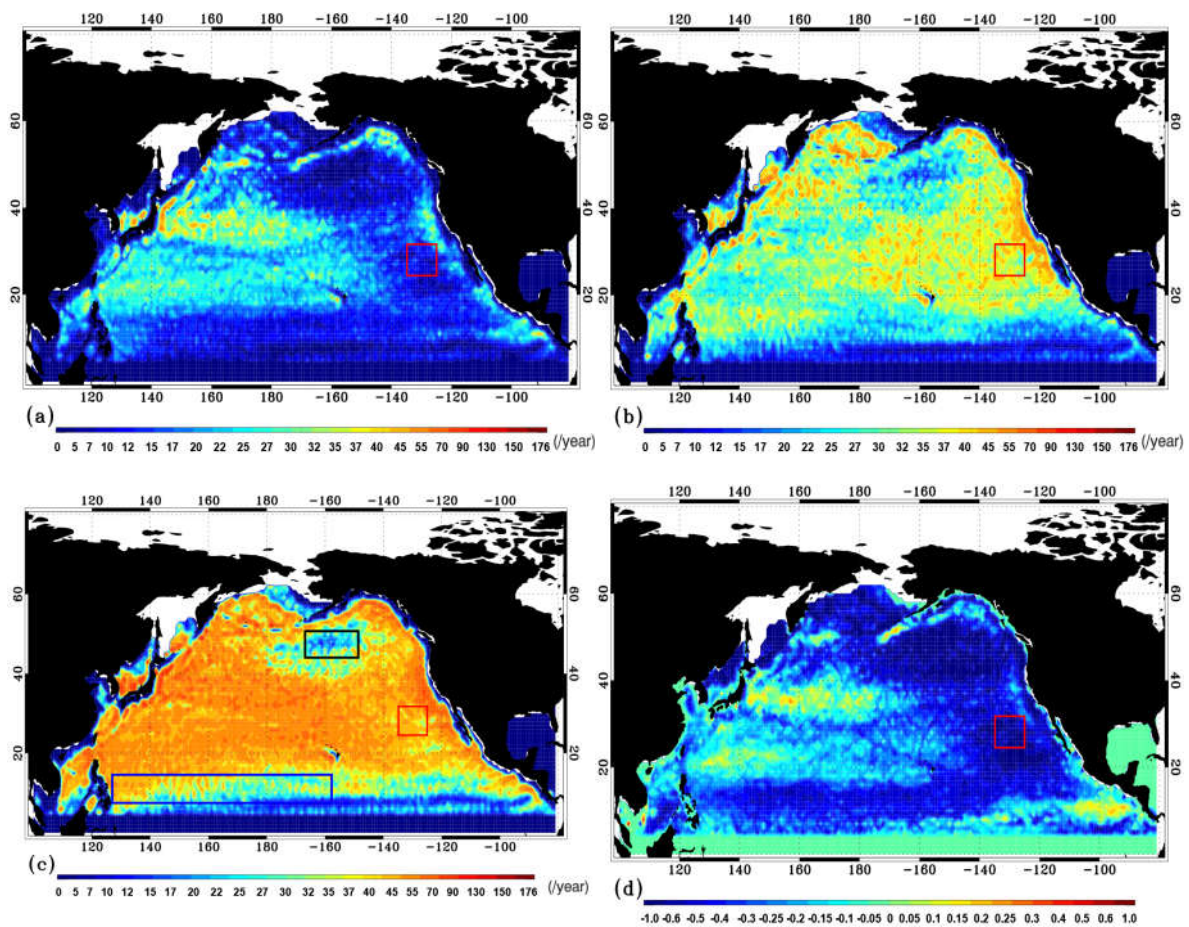
705

706

707

708

Figure 8. The logical genealogy of an ocean eddy with six states: birth, death, living, missing, splitting, and merging. (a) The logical relationships of eddies between two days. (b) The logical genealogy evolution model of an example eddy.



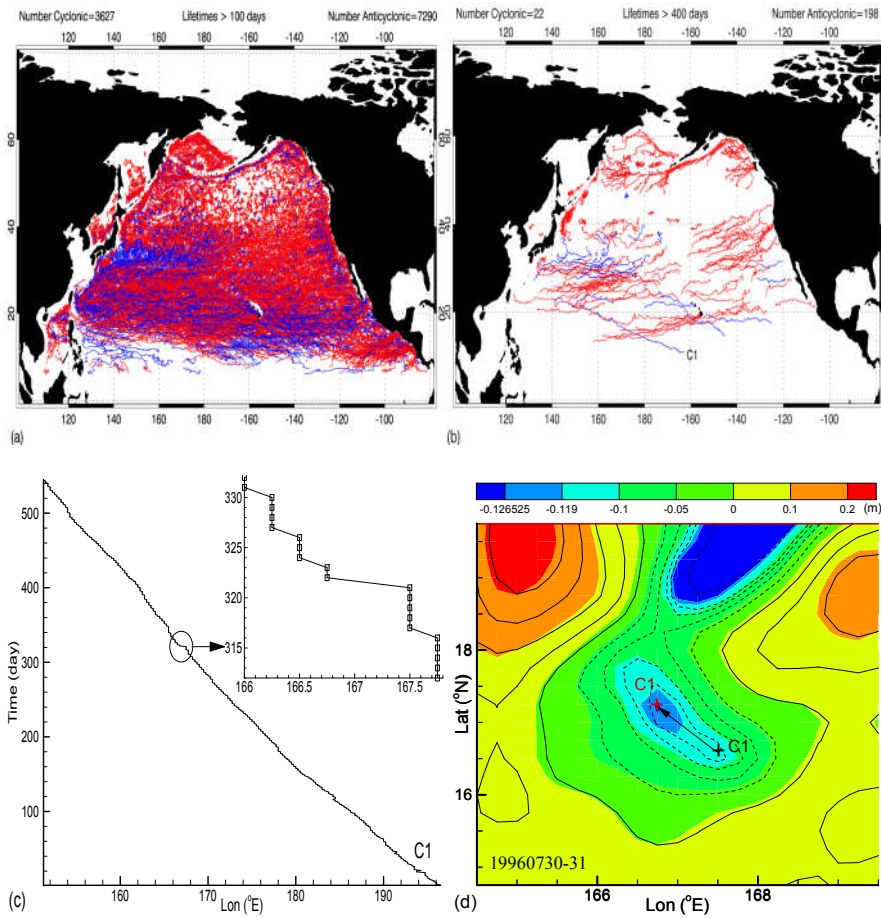
709

710

711 Figure 9 (a) The number of cyclonic eddy extrema on each  $1^\circ \times 1^\circ$  grid per year. (b) Same as (a), except for  
 712 anticyclonic eddies. (c) Same as (a), except for the total number of eddies. (d) The ratios of difference in number of  
 713 cyclonic and anticyclonic eddies to the total eddies (A logarithmic scale is used). The black box is the “eddy desert”,  
 714 the blue box is the NEC. The red boxes are the locations of merging/splitting examples in Figure 11, where  
 715 anticyclonic eddies dominated.

716

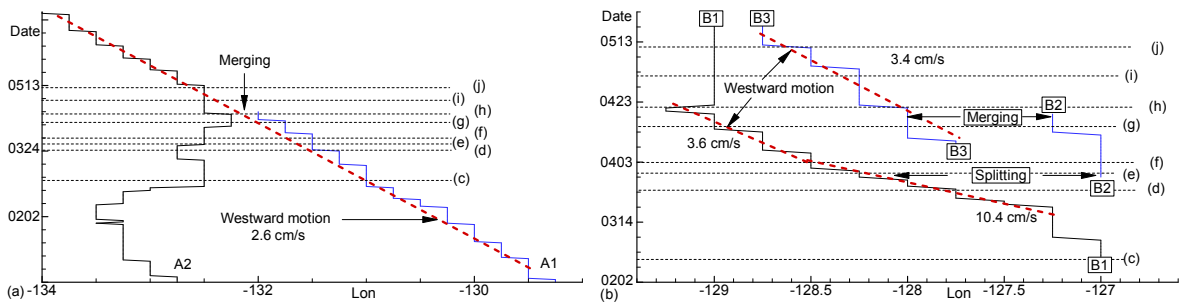
717



718

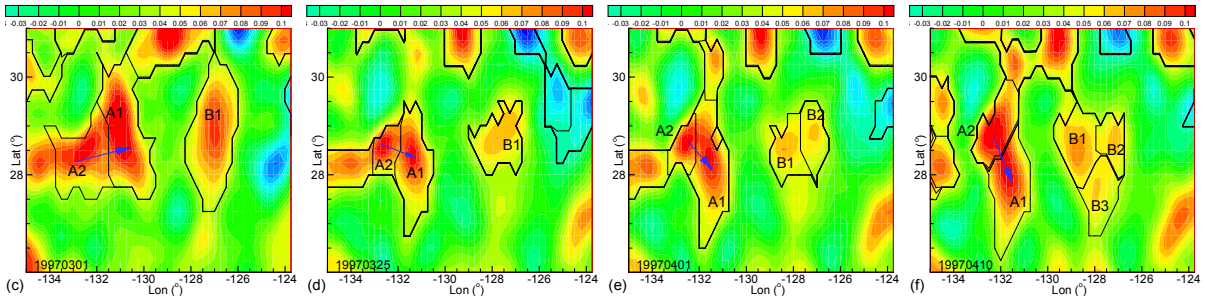
719 Figure 10. (a) Tracks of long-lived (>100 days) eddies. (b) Tracks of long-lived (>400 days) eddies. In (a) and (b),  
 720 blue color marks cyclonic eddies, and red color marks anticyclonic eddies. (c) The track of eddy C1. Note the  
 721 sudden jump from 167.5°E to 166.75°E on July 31, 1996. (d) The SLA fields on July 30 (contours) to 31 (shading),  
 722 using the same intervals for the contours and the shadings. The eddy centers are marked by a black cross (July 30)  
 723 and a red cross (July 31).

724

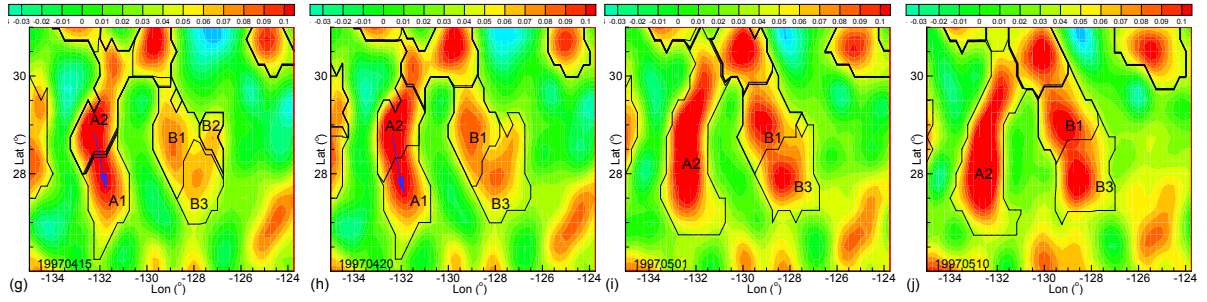


725

726



727

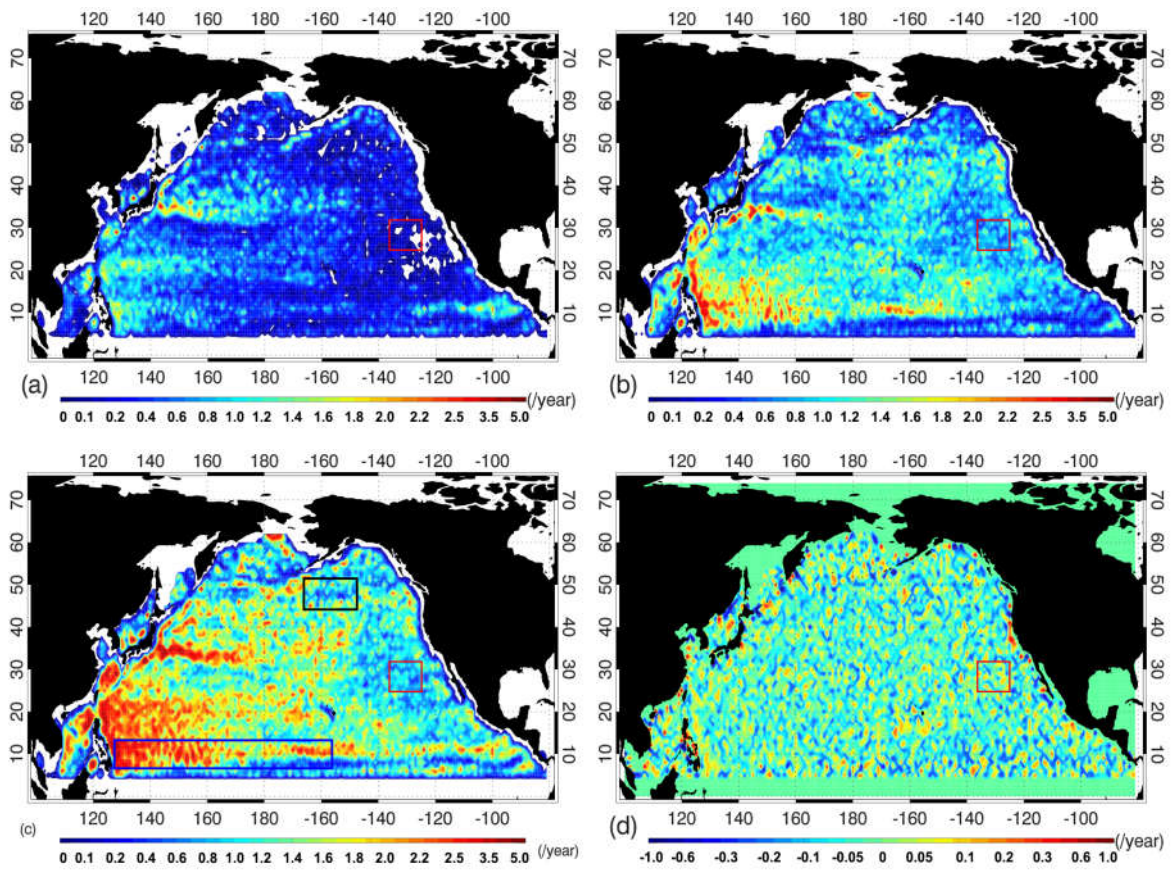


728 Figure 11. The dynamic evolutions of two groups of eddies, which are located in the red boxes in Fig. 9. (a) Two  
729 eddies, A1 and A2, approached each other, and A1 merged with eddy A2, where the blue arrows indicate that the  
730 eddy centers rotated clockwise during the merging process. (b) In the mean time, eddy B1 split into two small eddies.

731 (c)-(j) The evolutions of SLA fields and eddies. Note that eddies A1 and A2 had clockwise rotations when they  
732 approached each other, as indicated by the blue arrows in (c)-(h).

733

734



735

736

737

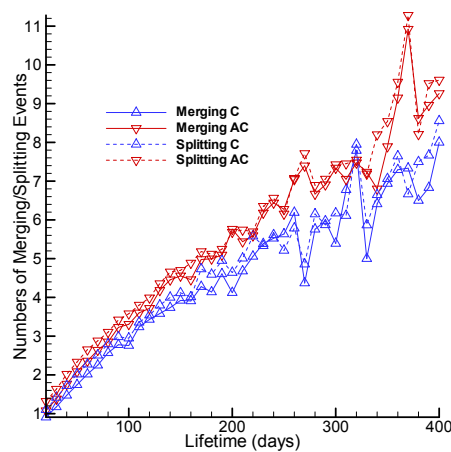
738

739

740

741

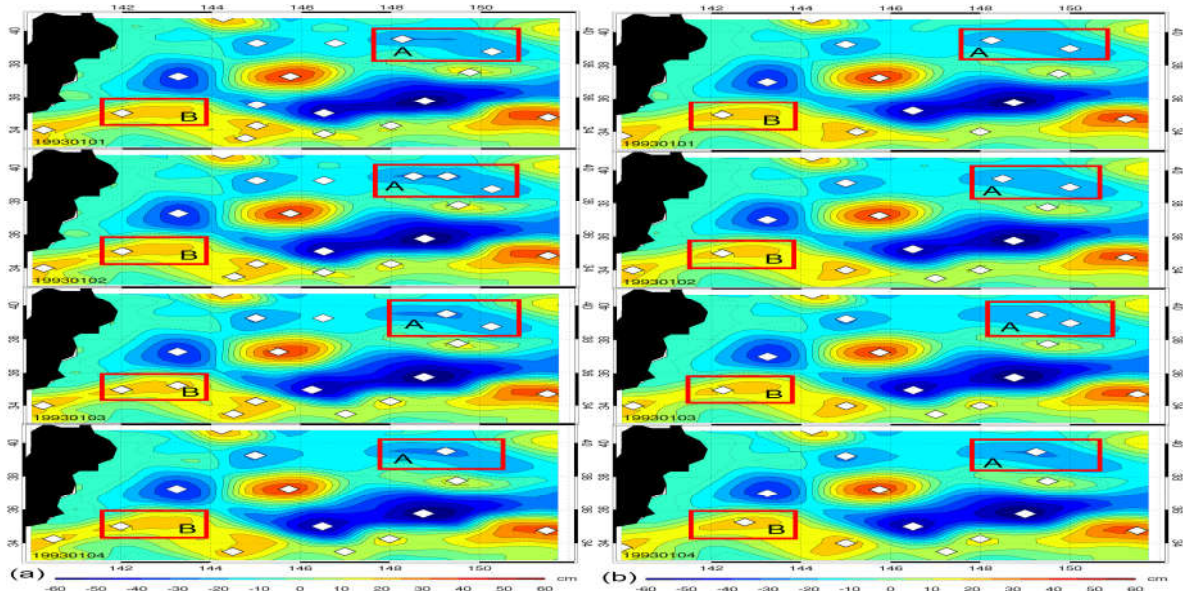
Figure 12. The frequencies of dynamic processes per  $1^\circ \times 1^\circ$  grid element. (a) The merging frequency for cyclonic eddies. (b) The merging frequency for anticyclonic eddies. (c) The merging frequency for all eddies. (d) The ratios of difference between the frequencies of merging and splitting for all eddies to the sum of merging and splitting frequencies for all eddies. The boxes are the same in Figure 9. The blue box is the location of NEC, where merging frequency is high.



742

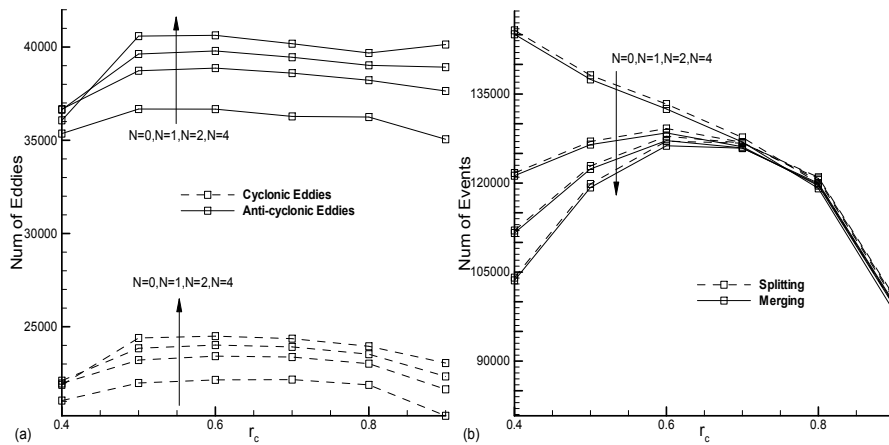
743 Figure 13. The number of merging/splitting events per eddy as function of eddy lifetime, where AC and C presents  
 744 anticyclonic and cyclonic eddies. The dynamic events are approximately linear increase with lifetime. The  
 745 merging/splitting events are more frequent for anticyclonic eddies than for cyclonic eddies.

746  
 747



748  
 749 Figure 14. Comparison of the non-smoothed (a) and smoothed SLA data (b) from January 1 to January 4, 1993,  
 750 where the color field shows SLA, white dots mark eddy centers, and two boxes A and B mark the regions sensitive  
 751 to noise. Note that small noise affected the eddy detection.

752



753  
 754 Figure 15. (a) Number of eddies (lifetime > 30 days) vs. the critical value  $r_c$  and look-ahead time  $N$ . (b) Number of  
 755 merging and splitting events vs. the critical value  $r_c$  and look-ahead time  $N$ .